



ISSN: 0067-2904

## Implementation of An Optical Gauss Meter Based on Ferrite and Hematite Ferrofluids

Sadeq H. Lafta <sup>1\*</sup>, Hussein T. Salloom <sup>2</sup>, Furqan S. Hashim <sup>3</sup>

<sup>1</sup>Applied Science department, University of Technology- Iraq, Iraq

<sup>2</sup>Al-Nahrain Renewable Energy Research Center, Al-Nahrain University, Iraq

<sup>3</sup>Mustansiriyah University, College of Dentistry, Iraq

Received: 12/2/2023 Accepted: 26/1/2024 Published: 30/9/2024

### Abstract

Three compositions  $Ni_{0.5}Fe_{2.5}O_4$ ,  $Ni_{0.7}Fe_{2.3}O_4$ , and  $Fe_2O_3$  were prepared by the co-precipitation method and checked by XDR, SEM, and VSM. The nanoparticles show a good match with the XRD standards. The particle sizes were 25, 32, and 18nm for the above compositions, respectively. The first composition showed the highest magnetization saturation. Suspensions containing the mentioned nanoparticles were prepared with two carrier fluids, distilled water, and dimethylsulphoxide (DMSO). A transmission to ultraviolet-visible light was tested and showed good transparency of more than 60 % in the red light region. The transparency to 623nm laser light under different magnetic fields of the six suspensions was tested. A simple device was fabricated to perform this test. The water suspension in water  $Ni_{0.5}Fe_{2.5}O_4$  has a larger variation in the transmitted power. The suspension of hematite shows no sensible change in the transmitted power. The magnetic properties of the nanoparticles and the dispersion property of the carrier fluid were behind the explanation of the suspension behaviours under the influence of the magnetic field.

**Keywords:** Ferrofluids; magneto-optics; ferrites; laser transmission, ferrite, hematite.

### تنفيذ كاوسميتر بصري بالاعتماد على المواع المغناطيسية للفيررات والهيماتيت

صديق هاني لفته<sup>1\*</sup>, حسين ثامر سلوم<sup>2</sup>, فرقان سالم هاشم<sup>3</sup>

<sup>1</sup>العلوم التطبيقية، الجامعة التكنولوجية، بغداد، العراق

<sup>2</sup>مركز النهرين للطاقة المتجددة، جامعة النهرين، بغداد، العراق

<sup>3</sup>كلية طب الاسنان، الجامعة المستنصرية، بغداد، العراق

### الخلاصة

تم تحضير ثلاثة مركبات  $Ni_{0.5}Fe_{2.5}O_4$  و  $Ni_{0.7}Fe_{2.3}O_4$  و  $Fe_2O_3$  (الهيماتيت) بطريقة الترسيب المشترك وفحصت الجسيمات النانوية بواسطة XDR و SEM و VSM. أظهرت الجسيمات النانوية تطابقاً جيداً مع معايير XRD. كانت أحجام الجسيمات 25 و 32 و 18 نانومتر للمركبات المذكورة أعلاه على التوالي، بينما أظهر التركيب الأول أعلى تشبع تمغنط. تم تحضير المعلمات المحتوية على الجسيمات النانوية المذكورة مع سائلين حاملين هما الماء المقطر وثنائي ميثيل سلفوكسيد (DMSO). وتم اختبار نفاذيتها للضوء المرئي وفوق البنفسجي وأظهرت شفافية جيدة بأكثر من 60% في منطقة الضوء الأحمر. كما تم اختبار

\*Email: [sadeqhlaftha@uotechnology.edu.iq](mailto:sadeqhlaftha@uotechnology.edu.iq)

الشفافية لضوء الليزر من 623 نانومتر بوجود مجال مغناطيسي مختلف القيمة للمعلقات الستة. حيث تم تصنيع جهاز بسيط لإجراء هذا الاختبار. النموذج العالق في الماء للمركب  $Ni_{0.5}Fe_{2.5}O_4$  يمتلك أكبر تباين في القدرة النافذة. بينما لا يُظهر عالق الهيماتيت أي تغيير معقول في القدرة النافذة. كانت الخصائص المغناطيسية للعينات والمحاليل وراء تفسير سلوكيات العوالق بوجود المجال المغناطيسي..

## 1. Introduction

Nanomaterials, especially nano ferrites, have acquired new applications [1-4]. Ferrites, bulk and nano, and iron oxides play a main role in different magnetic and electric applications [5,6]. Magnetic liquids, also called ferrofluids, are stable colloidal systems created when nano-grade magnetic particles are highly dispersed in some liquids [7-10]. Typically, ferrofluids consist of metals (Fe, Ni, or Co) or cubic spinel oxidic single-domain ferromagnetic ceramics suspended in water or organic solvents with suitable surfactants. With a controllable rheological property and sharp magnetic attraction, ferrofluids can earn diverse special physical, chemical, and magneto-optical properties [11]. Ferrofluids are used in loudspeakers, stepper motors, heat exchangers, and sensors [12]. Additionally, they have worked as a functional material in biomedicine applications [13].

Manipulating the optical properties of ferrofluids forced by magnetic fields is the subject of extensive research activities. The researchers targeted the integration of ferrofluids in an optical device such as optical shutters, attenuators, and polarizers, provided that particles remain mono-dispersible in a closed system and their movement is restricted in two dimensions [14-16]. Within this context, Nair et al. [11] utilized ferrofluid thin films belonging to the series  $Ni_xFe_{1-x}Fe_2O_4$  ( $Zn_xFe_{1-x}Fe_2O_4$ ) encapsulated between two glass slides as a Gauss meter for field and magnetic moment sensing. Mormile et al. [12] studied the propagation of light beam at the interface of prism-magnetic fluid film. They investigated the effects of the magnetic field on the refractive index of the magnetic fluid.

In this paper, three compositions of nickel ferrite ( $Ni_{0.5}Fe_{2.5}O_4$  and  $Ni_{0.7}Fe_{2.3}O_4$ ) and hematite  $Fe_2O_3$  were prepared as a suspension in distilled water and dimethylsulphoxide (DMSO). Their optical properties were investigated using UV-visible spectroscopy. The Six suspensions were tested for their transparency to 623nm laser light at different magnetic fields.

Sensing and measuring the magnetic field is significant in orientation, navigation, memory, recording media, scientific research (spectroscopy, nuclear, particle physics, optics, and even rheology), industrial applications, and biomedical (like those used in magnetic resonance and biosensors). From this point, this work is trying to use Ni ferrite and hematite ferrofluids as a sensing element for different magnetic fields.

## 2. Experimental work

### 2.1. Ferrofluid preparation

The compositions  $Ni_{0.5}Fe_{2.5}O_4$  and  $Ni_{0.7}Fe_{2.3}O_4$  were synthesized by the co-precipitation method using  $FeCl_3$  and  $NiCl_2.6H_2O$  in a stoichiometric weight ratio. NaOH was added to reach a pH of about 8. The solutions were heated to about 90°C. The resulting suspensions were washed four times with distilled water, followed by drying at 70°C in the oven to produce the final powder. The same procedure was conducted to prepare the hematite phase, except no  $NiCl_2.6H_2O$  was used. The powders were examined with an X-ray diffractometer (XRD) (Shimadzu-6000), scanning electron microscope (SEM) (LEO-1450), and vibrating sample magnetometer (VSM) (MDK at Iran Kashan University).

The magnetic fluids were prepared by mixing the prepared nano powder iron oxide (hematite,  $Fe_2O_3$ , or Ni ferrites) with distilled water or dimethylsulphoxide (DMSO). For the

Ni ferrite with the  $\text{Ni}_x\text{Fe}_{3-x}\text{O}_4$  structure,  $x$  was chosen to be 0.5 and  $x=0.7$  to obtain  $\text{Ni}_{0.5}\text{Fe}_{2.5}\text{O}_4$  and  $\text{Ni}_{0.7}\text{Fe}_{2.3}\text{O}_4$ . 5 mg of each of the prepared nanopowders (weighted by a sensitive 4.0-digit balance) were separately dissolved in 2 ml of distilled water and DMSO, respectively. The mixing process was performed in an ultrasonic bath for one hour. UV-Vis spectrophotometer (Sigma, USA) was used to determine the transmittance of all samples in the wavelength range (190–1100 nm).

## 2.2. Lab-built experimental setup

### 2.2.1. The coils

A lab-built solenoid of two coils 0.5cm apart was used to produce a uniform variable magnetic field. The coils were of copper wire wound around a clear transparent polyethylene cylinder, which has a hole drilled between the coils to install the sample, as shown in Figure 1a. Each coil is 280 turns with an average diameter of 0.5cm, 3cm coil length, and a wire thickness of about 0.8mm. A power supply of 30V with a 5A current was used to supply the coils with current. The diameter of the index in both parts of the coil is almost equal; the slight variation in length and diameter does not affect the magnetic field uniformity and its calculation between the two coils because the coils, generally, achieve the condition of Helmholtz for a uniform field (coil diameter equals the distance between the two coils). Calibration of the magnetic field generated at the centre of the two coils versus current changes was performed utilizing a commercial Gauss meter (NV621). It is worth noting that the fabricated coils could withstand a current greater than 5A, and can exceed this value by providing a cooling fan.

### 2.2.2 .Optical Gauss meter

As shown in Figure1, the proposed Gauss meter consists of laser light as a light source, a ferrofluid sample, and a homemade powermeter (photodetector, and the 3-digit display). A wooden panel was used for setting the experimental arrangement. The laser diode with a wavelength of 623nm and power of 2.5mW was chosen as a light source. This laser diode is available locally at a reasonable cost and performs the desired purpose. The laser light power was detected by the homemade power meter consisting of a photodetector (OPT101), which is a monolithic photodiode with an on-chip trans-impedance amplifier operating from +2.7V to +36V. A digital voltmeter having a 3-digit display, which means a wide precise range of readings (HR0201-1 Mini) was connected to measure the output voltage from the detector. A shielding tube of 0.5 cm diameter was placed vertically to the detector to prevent the ambient light of the laboratory from reaching the detector. The magnetic field was produced by two Helmholtz coils as given in section 2.2.1.

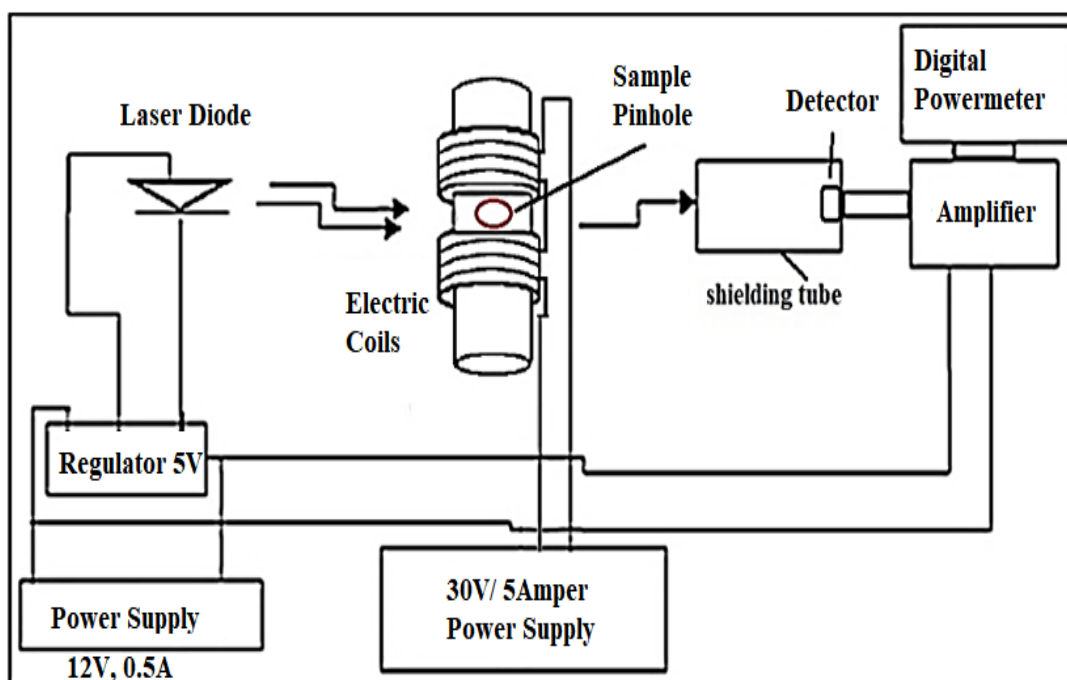


**Figure.1:** Optical Gauss meter circuit and setup block diagram.

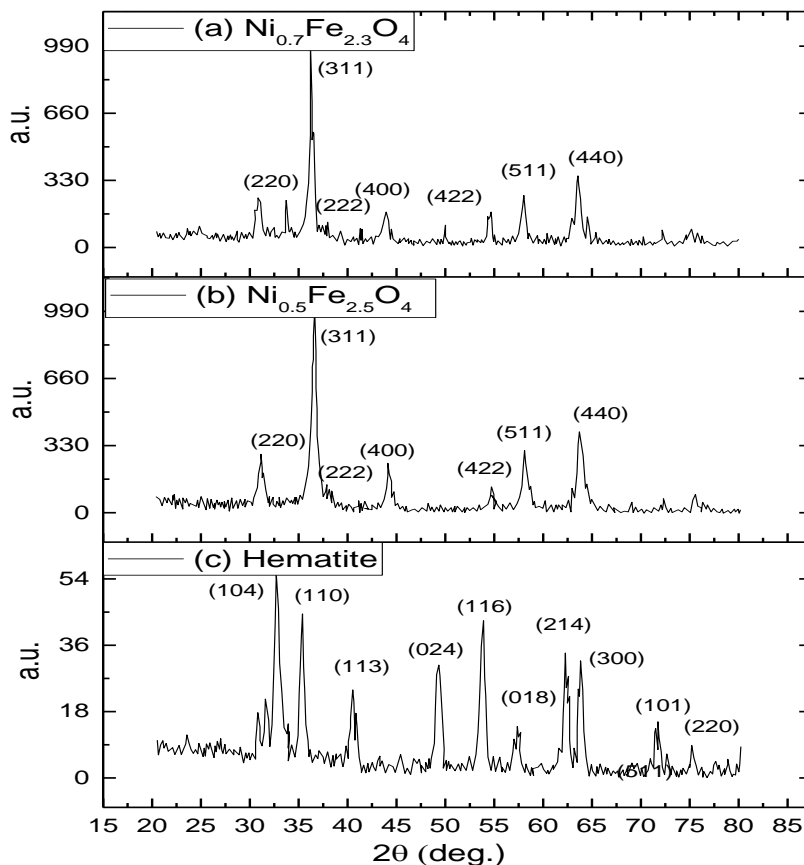
A power supply of 12V voltage with a maximum current of 0.5A was used to drive the circuits. A voltage regulator (8MO5B regulator) was installed to regulate the 12V voltage to around 5V suitable to drive the laser diode.

In the experimental setup, a ferrofluid sample in a capillary glass tube of 2mm inner diameter is put between the two coils, which were used to generate the magnetic field. The sample tube was placed in the uniform field area between the coils, and its length was aligned normally to the magnetic field direction. The laser beam from the laser diode was allowed to pass normally through the ferrofluid sample. The laser power was carefully aligned with the detector to reach the highest possible readings when there was no sample at a detector-diode laser distance of about 15 cm. This voltage increases linearly with the light intensity falling on the detector.

### 3. Results and discussion

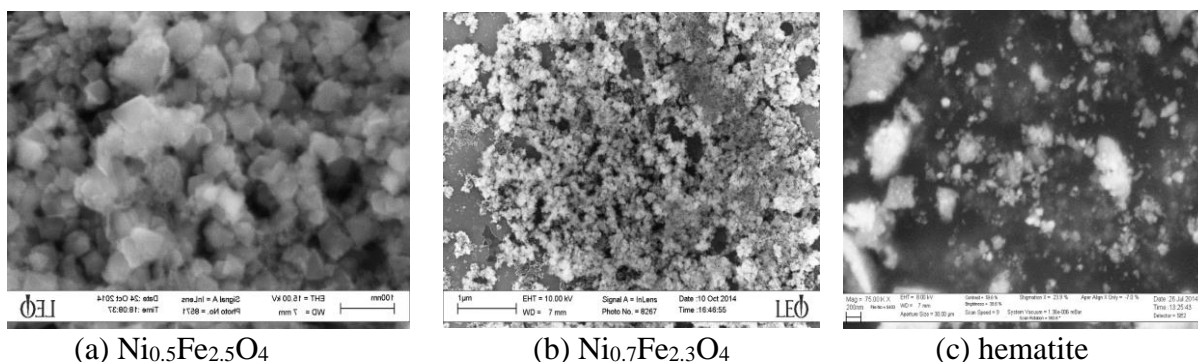
#### 3.1 Structural and morphological analysis

Figure (2) illustrates the XRD patterns of the prepared samples. The XRD scanning range of  $2\theta$  was  $20^\circ$ – $80^\circ$ , which contains the most intensive peaks in the spinel structure. The peaks located beyond  $80^\circ$  are weaker than those in the mentioned range [15,17]. Phase analysis was conducted by high score analysis. The  $\text{Ni}_{0.5}\text{Fe}_{2.5}\text{O}_4$  and the  $\text{Ni}_{0.7}\text{Fe}_{2.3}\text{O}_4$  samples had a reasonable match with Ni ferrite, which belonged to space group  $\text{Fd}\bar{3}\text{m}$  [18-20], as shown in Figure 2(a) and (b), where the matching involved the planes (220), (311), (222), (400), (422), (511) and (440). The non-exact matching peaks with the spinel structure belonged to small residuals of NaCl and hematite. These peaks were cited at around  $32^\circ$ ,  $33.1^\circ$ ,  $41.5^\circ$ , and  $49.5^\circ$ . Figure 2(c) shows the XRD pattern of the prepared hematite nanoparticles with a good matching with the rhombohedral crystal structure with the  $\text{R}\bar{3}\text{c}$  space group [21]. This Figure clearly shows the matching between the pattern and the rhombohedral planes (104), (110), (113), (024), (116), (018), (214), (300), (101), and (220).



**Figure 2:** The XRD patterns of (a)  $\text{Ni}_{0.5}\text{Fe}_{2.5}\text{O}_4$ , (b)  $\text{Ni}_{0.7}\text{Fe}_{2.3}\text{O}_4$ , and (c) Hematite.

Figure3 displays the SEM images for the three samples. All images show that the three samples have particles with nearly a spherical shape and a clear agglomeration. The particle sizes were 25nm, 32nm, and 18nm for  $\text{Ni}_{0.5}\text{Fe}_{2.5}\text{O}_4$ ,  $\text{Ni}_{0.7}\text{Fe}_{2.3}\text{O}_4$ , and Hematite, respectively. Some particles showed a polyhedral shape due to their crystallite size being very close to the particle size, as shown in Figure3(a). Hematite, in Figure3(c), showed less agglomerations compared to the ferrite particles, Figure3(a) and (b), because hematite particles generally have a lower magnetic moment (saturation magnetization) compared to the ferrite particles.



**Figure 3:** The SEM images of the prepared nanoparticles for (a)  $\text{Ni}_{0.5}\text{Fe}_{2.5}\text{O}_4$ , (b)  $\text{Ni}_{0.7}\text{Fe}_{2.3}\text{O}_4$ , and (c) Hematite

### 3.2 Magnetic analysis

Figure4 shows the hysteresis loops of the three magnetic synthesized nanoparticles. The ferrites  $\text{Ni}_{0.5}\text{Fe}_{2.5}\text{O}_4$  and  $\text{Ni}_{0.7}\text{Fe}_{2.3}\text{O}_4$  show the usual soft loop with a slight coercive field, while hematite displays an unsaturated curve. When  $x$  is changed from 0.5 to 0.7,  $\text{Ni}^{2+}$  ions

occupy octahedral sites governed by ionic radius. It begins to push  $\text{Fe}^{3+}$  to tetrahedral sites, causing opposite moments at octahedral sites. The drop in the saturation magnetization ( $M_s$ ) within the range ( $x=0.5 - 0.7$ ) is due to a decrease in  $\text{Fe}^{3+}$  at the octahedral site (B), which reduces A-B interaction and, therefore,  $M_s$  [22]. All samples are thought to exhibit super-paramagnetic activity depending on the s-shape of the loops. These behaviors belong to different reasons, such as different phases, those of ferrites and hematite, super-paramagnetic state, and redistribution of cations. This is usually associated with very low coercivity ( $<50\text{Oe}$ ) and particle size ( $<30\text{ nm}$ ) [23] for ferrites. It was found that the reduction in magnetic coercive force ( $H_c$ ) was mainly due to the decrease in particle size [24].

The sample with maximum  $M_s$  has a maximum value of remanence magnetization  $M_r$  and initial permeability  $\chi_i$  because of the dependence of the latter parameters on the former one. Saturation magnetization values of ferrite-based nanoparticles are lower than those of bulk material ( $55\text{ emu/g}$ ) [25]. Here, the  $\text{Fe}^{3+}$  and  $\text{Ni}^{2+}$  cations content and their distribution are responsible for the magnetism. The  $\text{Ni}^{2+}$  ions prefer octahedral sites, and  $\text{Fe}^{3+}$  is cited over octahedral and tetrahedral sites [26].

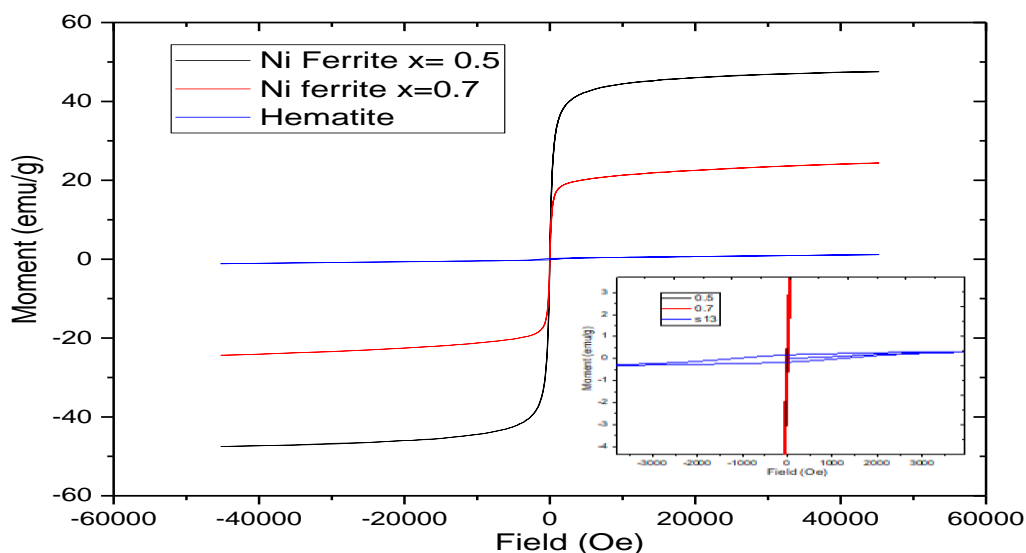


**Figure 4:** The magnetic hysteresis loops of the prepared nanoparticles.

Table.1 Some structural magnetic parameters of saturation magnetization for the prepared samples.

**Table 1:** Some structural and magnetic parameters of the prepared particles

Material	Crystallite size nm	Average particle size nm	Saturation Magnetization $M_s$ (emu/g)	Magnetic coercive force $H_c$ (Oe)	Initial Permeability $\chi_i$ emu/g.Oe	Remanence magnetization $M_r$ emu/g
$\text{Ni}_{0.5}\text{Fe}_{2.5}\text{O}_4$	16	22	57	4	1.3	0.4
$\text{Ni}_{0.7}\text{Fe}_{2.3}\text{O}_4$	27	35	26	27.3	0.26	1.7
Hematite	14	20	unsaturated	1375	$9.8 \times 10^{-5}$	0.17

### 3.3 Calibration the power of the proposed optical gauss meter

Figure(5) illustrates the calibration of the fabricated power meter of the optical Gauss meter compared to a standard light power meter (Sanwa power meter/Japan).

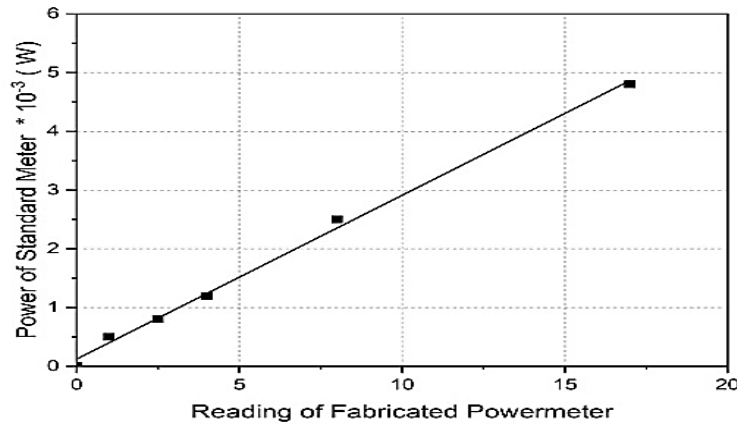


**Figure 5:** The calibration curve of the fabricated power meter of the optical Gauss meter with a standard light power meter.

The device’s working mechanism can be summarized as follows: the red laser light source passes through the sample, which is influenced by the magnetic field generated by the coils. Then the laser beam is received by the photo-detector and a digital voltmeter to measure its modified power. The power with no sample was previously measured. The coils are connected in series with the power supply to generate the variable magnetic field according to applied voltage and current. The laser incident on the detector surface induces an electric current that is transformed into a voltage signal at the output of the detector. This is amplified by the amplifier, which can be measured by the digital voltmeter. Any variation in laser intensity will be displayed as a readable digital voltage value. The changes in the magnetic field (generated by the coils) produce variations in the power of the laser output from the samples.

### 3.4 Calibration of the magnetic field in terms of coil current and distance

It is well-known that the magnetic field intensity (H) generated by the coils depends on the current (I) passing through the coils, number of coil turns (N), and inversely on the coil length (L), according to  $H = \mu_0 N I / L$  [27], where  $\mu_0$  is the permeability of the free space. Figure 6(a) shows a linear relationship between the produced magnetic field and the current passing through the solenoid. As the magnetic field is in Tesla units, according to the used tesla-meter, this unit need to be converted to Ampere per meter (A/m) via dividing by ( $\mu_0$ ) permeability of vacuum. Figure 6(b) shows the magnetic field induction (flux density) dependence on the distance (d) between the two coils. The relationship between the magnetic field (H) and the coil current is also linear.

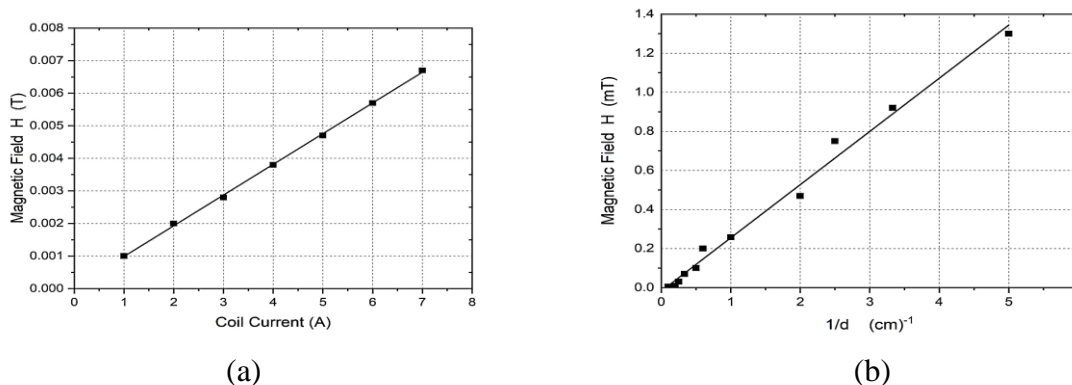


**Figure 6:** The magnetic field changes with (a) coil current and (b) distance.

### 3.5 UV- Visible optical properties of the suspension

Figure 7 shows the UV-Vis transmission spectra of the three sample suspensions. It is clear that the samples have good transmission to the wavelength (623nm), it exceeded (65%) for the three samples.

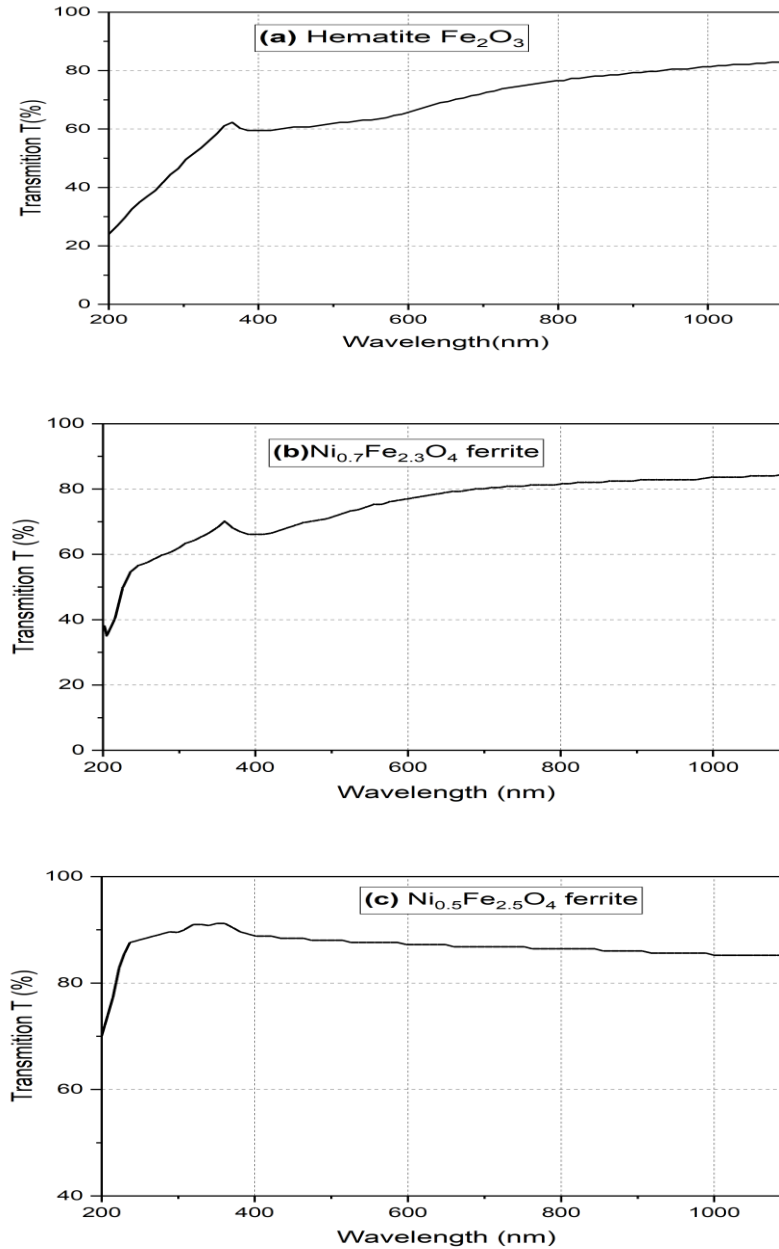


**Figure 7:** UV-visible transmission spectra of the prepared suspensions. (a) Hematite  $Fe_2O_3$ , (b)  $Ni_{0.7}Fe_{2.3}O_4$  ferrite, and (c)  $Ni_{0.5}Fe_{2.5}O_4$  ferrite

### 3.6 Laser transmission as a function of the applied magnetic field.

The laser output power of the water-suspended magnetic liquids as a function of magnetic field intensity was collected by the photodetector, and the corresponding electric signal was displayed by a digital voltmeter. Figure 8 depicts the change in light power versus magnetic field intensity for the water-suspended magnetic liquids. At the beginning of the magnetic field increase, the transmitted power increased sharply, and then it increased slowly to a stable value. Figure 8(a), for the sample  $Ni_{0.7}Fe_{2.3}O_4$ , shows an increase in the transmitted power

from 0 to about 2.5mW as the magnetic field increased from 0 to about 15mT. This behavior is also shown in Figure8(b) for the sample  $\text{Ni}_{0.5}\text{Fe}_{2.5}\text{O}_4$  suspended in water where the transmitted power reaches about 2.5mW at the field of value of 4.5mT. The reason can be explained by the attraction and moving of the magnetic particles to regions of high field strength, resulting in a reduction of light scattering with the increase of the applied field due to the decrease in particle cluster formation. So, as in the weak field, the relation of the output laser intensity with the applied field is almost linear. But as the particle cluster gets smaller or even vanishes in higher fields, output transmitted laser intensity also tends to a saturated value. In Figure8(c) for the hematite  $\text{Fe}_2\text{O}_3$  sample, there is no observed variation in the transmitted power. This can be related to the poor magnetization of this material, which is already classified as weak ferromagnetic. It has been suggested that the reaction of nanofluids to applied magnetic fields may be connected to their anisotropic microstructure and chain-like alignments [28]. Magnetite nanoparticles having a diameter ( $d$ ) and effective susceptibility ( $\chi$ ) gain induced dipole moments ( $m$ ) in the presence of an external magnetic field ( $H$ ), and its magnitude as given by [29,30]:

$$m = \frac{\pi}{6} d^3 \chi H \quad (1)$$

If the exterior magnetic field grows in stages, the nanoparticle moments tend to coordinate along the field direction, creating doublets, triplets, and small chains-like structures. Magnetic nanoparticles thus form chain-like structures when exposed to the external magnetic field [31].

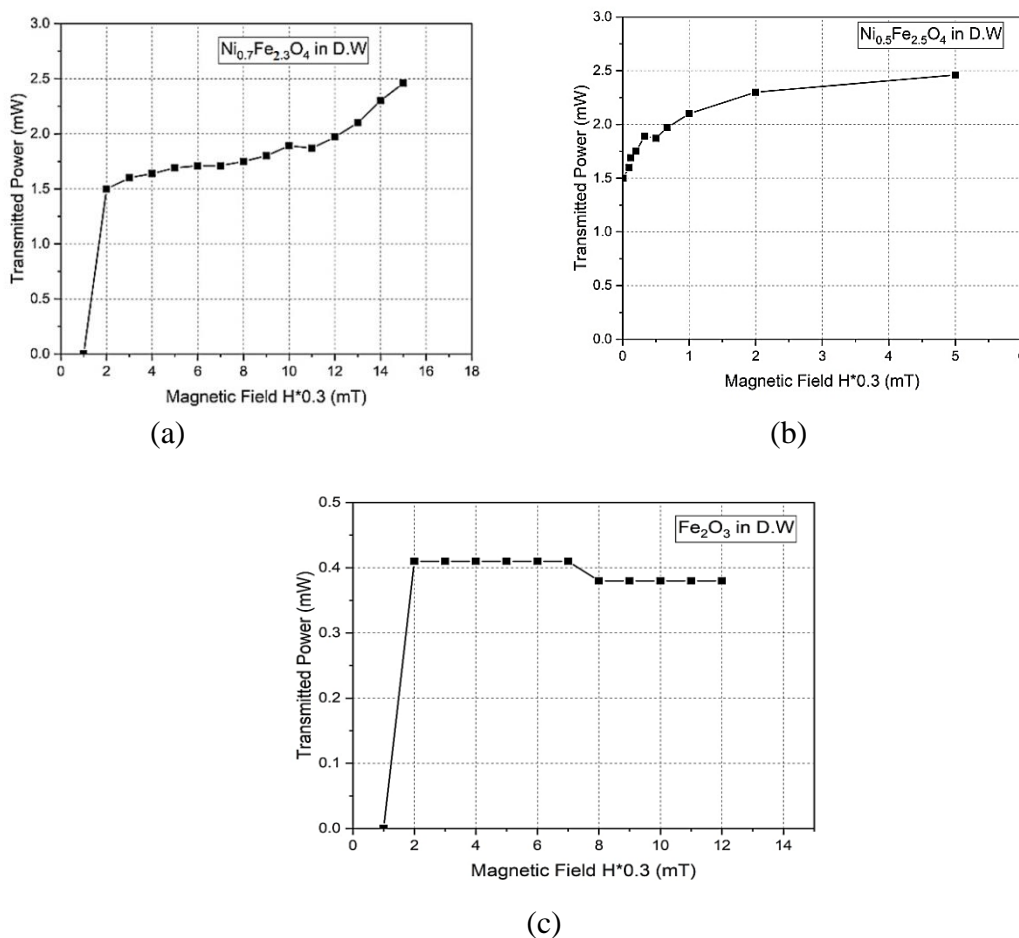


**Figure 8:** The transmitted power of the laser from sample suspensions in water.

Figure 9 shows the variation of laser transmitted for the same samples suspended in DMSO. It was found that most of the particles were collected at the bottom of the capillary glass tube, allowing light to be scattered resulting in higher variation in the light passing through it.

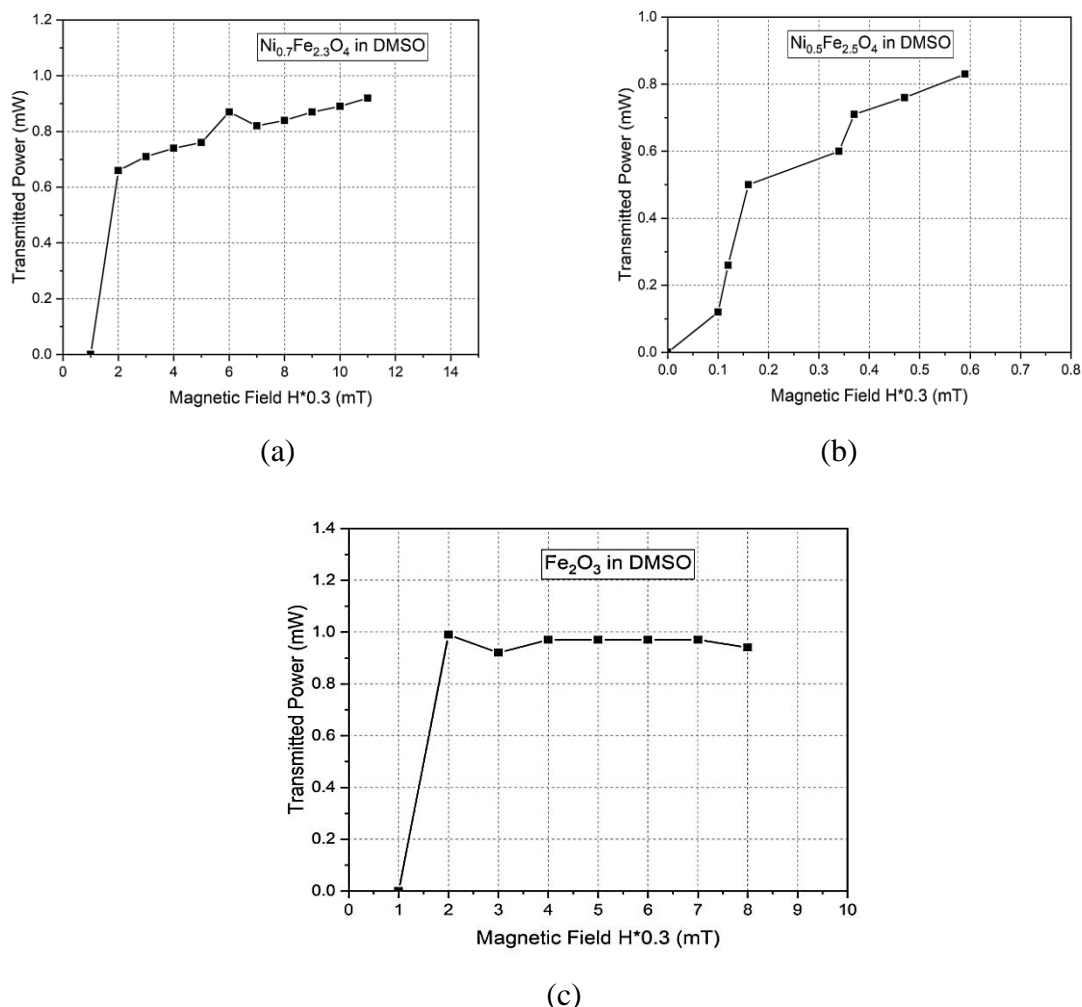


**Figure 9:** Laser transmitted power for the sample suspensions in DMSO. (a) For  $\text{Ni}_{0.7}\text{Fe}_{2.3}\text{O}_4$  nanoparticles, (b) For  $\text{Ni}_{0.5}\text{Fe}_{2.5}\text{O}_4$  nanoparticles, and (c) For Hematite nanoparticles.

The transmitted power through the  $\text{Ni}_{0.5}\text{Fe}_{2.5}\text{O}_4$  sample is slightly higher than that for  $\text{Ni}_{0.7}\text{Fe}_{2.3}\text{O}_4$  due to its magnetic properties. The amount of change in the transmitted power is generally higher in water by 2.5 times than in DMSO because the dispersion power is higher for DMSO than that of deionized water. Also, the mobility of the particles in water resulted from lower viscosity, i.e. the rotation of the magnetic particles in deionized water is easier than in the DMSO material. This may be due to the viscosity of water (1.0016 mPa.s at 20°C) and that of DMSO (.5 mPa.s at 20°C) [32]. As the liquid viscosity increases, the friction with particles increases. This will require higher shear stress, stimulated by the magnetic field, for rotating the particles in DMSO.

#### 4. Conclusions

The nano Ni ferrite compositions  $\text{Ni}_{0.5}\text{Fe}_{2.5}\text{O}_4$  and  $\text{Ni}_{0.7}\text{Fe}_{2.3}\text{O}_4$  can change the laser power of wavelength 623nm under the change in the applied magnetic field. This enables using the proposed device with the applied suspensions for magnetic field intensity measuring based on

the calibration curves of magnetic field intensity. The liquid matrix plays an important role in the range of the possible reading values and the accuracy of each reading.

Conflict of Interest: The authors declare that they have no conflicts of interest.

### References:

- [1] H. T. Salloom, T. K. Hamad, & F. H. Rajab, "Laser-Induced Breakdown Spectroscopy for Determination of Toxic Metals in Fertilizers: emphasis on Lead," *Iraqi Journal of Science*, vol. 63, no. 7, pp. 2523–2531, 2022, <https://doi.org/10.24996/ij.s.2022.63.6.19>
- [2] M. F. Al-Hilli, "A comparison study of the structural and magnetic properties of pure Ni metal and NiZnMn ferrite," *Iraqi Journal of Physics*, vol. 17, no. 43, pp. 18–25, 2019, <https://doi.org/10.30723/ijp.v17i43.418>
- [3] K. R. Gbashi, A. Bahari, & S. H. Lafta, "Thin films for nano-electronics applications based on BaCaTiO<sub>3</sub>–SrZnTiO<sub>3</sub> perovskite with Au electrodes," *Applied Physics A*, vol. 129, article no. 350, 2023, <https://doi.org/10.1007/s00339-023-06621-1>
- [4] S. I. Ibrahim, S. H. Lafta, & W. A. Hussain, "Impact strength of surface treated SS316L wires reinforced PMMA," *Journal of the Mechanical Behavior of Materials*, vol. 30, no. 1, pp. 272–278, 2021, <https://doi.org/10.1515/jmbm-2021-0029>
- [5] M. F. A. Hilli, "Structural and electrical properties of Cu<sub>1-x</sub>La<sub>x</sub>Fe<sub>2</sub>-yO<sub>4</sub> ferrites," *Iraqi Journal of Physics*, vol. 11, no. 22, pp. 102–109, 2019, <https://doi.org/10.30723/ijp.v11i22.358>.
- [6] A. Ali, T. Shah, R. Ullah, P. Zhou, M. Guo, M. Ovais, Z. Tan, & Y. Rui, "Review on recent progress in magnetic nanoparticles: synthesis, characterization, and diverse applications," *Frontiers in Chemistry*, vol. 13, no. 9, p. 629054, 2021. <https://doi.org/10.3389/fchem.2021.629054>
- [7] M. Imran, A. R. Ansari, A. H. Shaik, A. Anas, S. Hussain, A. Khan, & M. R.Chandan, "Ferrofluid synthesis using oleic acid coated Fe<sub>3</sub>O<sub>4</sub> nanoparticles dispersed in mineral oil for heat transfer applications," *Materials Research Express*, vol. 5, no. 3, p. 036108, 2018, <https://doi.org/10.1088/2053-1591/aab4d7>
- [8] M. F. Al-Hilli, "Characteristics of AC. conductivity and dielectric behavior of CU<sub>0.5</sub> TI<sub>0.5</sub> HOX FE<sub>2</sub>-X O<sub>4</sub> ferrites," *Iraqi Journal of Science*, vol. 57, pp. 2245–2251, 2016, <http://www.iasj.net/iasj?func=fulltext&aId=121031>
- [9] S. H. Lafta, "Microwave losses of nanostructure Li-Ni ferrites in X-band and Ku-band," *Iraqi Journal of Physics*, vol. 14, no. 29, pp. 44–54, 2019, <https://doi.org/10.30723/ijp.v14i29.221>
- [10] C. Fan, E. Liang, & J. Huang, "Optical properties of one-dimensional soft photonic crystals with ferrofluids," *Frontiers of Physics*, vol. 8, no. 1, pp. 1–19, 2013, <https://doi.org/10.1007/s11467-013-0280-5>
- [11] S. S. Nair, S. Rajesh, V. Abraham, & M. R. Anantharaman, "Ferrofluid thin films as optical gaussmeters proposed for field and magnetic moment sensing," *Bulletin of Materials Science*, vol. 34, no. 2, pp. 245–249, 2011, <https://doi.org/10.1007/s12034-011-0059-7>
- [12] P. Mormile, L. Petti, M. Rippa, J. Guo, W. Song, & J. Zhou, "Magnetically modulated refractive index of a magnetic fluid film based on cigar-shaped ferrite submicron particles," *Proceedings of the SPIE*, vol. 7847, id. 78470C, 2010, <https://doi.org/10.1117/12.873419>
- [13] C. Scherer, & A. M. F. Neto, "Ferrofluids: properties and applications," *Brazilian Journal of Physics*, vol. 35, no. 3a, pp. 718–727, 2005, <https://doi.org/10.1590/s0103-97332005000400018>
- [14] L. Sun, S. Jiang, & J. R. Marciante, "All-fiber optical magnetic-field sensor based on Faraday rotation in highly terbium-doped fiber," *Optics Express*, vol. 18, no. 6, p. 5407, 2010, <https://doi.org/10.1364/oe.18.005407>
- [15] R. A. Ali, H. A. Yusr, & S. S. Bassam, "The magnetic switch manufacturing by using ferrofluid and ferrofluid doped copper nanoparticles," *Iraqi Journal of Physics*, vol. 18, no. 46, pp. 39–45, 2020, <https://doi.org/10.30723/ijp.v18i46.511> <https://ijp.uobaghdad.edu.iq/index.php/physics/article/view/511>
- [16] S. H. Lafta, "Broadband ferromagnetic resonance of non-stoichiometric nano Nickle ferrite with different Ni<sup>2+</sup> content," *Materials Research Express*, vol. 6, no. 4, p. 046103, 2019, <https://doi.org/10.1088/2053-1591/aafb80>

- [17] S. H. Lafta, "Impact of Ni<sup>2+</sup> Content on broadband Ferromagnetic resonance of superparamagnetic Ni ferrite (Having Fe<sup>2+</sup>)-Epoxy composite," *IEEE Transactions on Magnetics*, vol. 54, no. 9, pp. 1–8, 2018, <https://doi.org/10.1109/tmag.2018.2839731>
- [18] L. H. Abdel-Mohsen, S. H. Lafta, & M. Hashim, "Comparing the role of NaOH and NH<sub>4</sub>OH on structural and magnetic properties of spinel Ba ferrite synthesized by autocombustion method," *Journal of Physics*, vol. 2322, no. 1, p. 012081, 2022, <https://doi.org/10.1088/1742-6596/2322/1/012081>
- [19] L. H. Abdel-Mohsen, S. H. Lafta, & M. S. Hashim, "Magnetic properties of Ba Ferrite Substituted by Low Fraction of Ni Cations," *Kuwait Journal of Science*, vol. 50, no. 3A, pp. , 2023, <https://doi.org/10.48129/kjs.20239>
- [20] E. K. Al-Shakarchi, S. H. Lafta, A. M. Musa, M. Farle, & R. Salikhov, "The FMR behaviour of Li–Ni ferrite prepared by hydrothermal method," *Journal of Superconductivity and Novel Magnetism*, vol. 30, no. 9, pp. 2575–2579, 2017, <https://doi.org/10.1007/s10948-017-4058-9>
- [21] S. H. Lafta, A. A. Taha, M. M. Farhan, & S. Y. Abdulfattah, "Biocompatibility study of α-Fe<sub>2</sub>O<sub>3</sub> nanoparticles prepared by hydrothermal method," *Surface Review and Letters*, vol. 26, no. 09, p. 1950058, 2019, <https://doi.org/10.1142/s0218625x19500586>
- [22] S. H. Lafta, "Hydrothermal Temperature Influence on Magnetic and FMR Properties of Hematite Nanoparticles," *Surface Review and Letters*, vol. 29, no. 07, p. 2250096, 2022. <https://doi.org/10.1142/s0218625x22500962>
- [23] P. N. L. Lens, J. Virkutyte, V. Jegatheesan, Seung-Hyun Kim, S. Al-Abed, "Nanotechnology for water and wastewater treatment. Water Intelligence Online," vol. 12, IWA Publishing, 2013, <https://doi.org/10.2166/9781780404592>
- [24] N. Zhuo, N. Zhang, T. Jiang, P. Chen, & H. Wang, "Effect of particle sizes and mass ratios of a phosphor on light color performance of a green phosphor thin film and a laminated white light-emitting diode," *RSC Advances*, vol. 9, no. 47, pp. 27424–27431, 2019, <https://doi.org/10.1039/c9ra05503g>
- [25] K. Nejati, & R. Zabihi, "Preparation and magnetic properties of nano size nickel ferrite particles using hydrothermal method," *Chemistry Central Journal*, vol. 6, article number 23, 2012. <https://doi.org/10.1186/1752-153x-6-23>
- [26] K. Kamishima, T. Mashiko, K. Kakizaki, M. Sakai, K. Watanabe, & H. Abe, "Synthesis and magnetic characterization of Sr-based Ni<sub>2</sub>X-type hexaferrite," *AIP Advances*, vol. 5, no. 10, pp. ??, 2015, <https://doi.org/10.1063/1.4934792>
- [27] Y. Khairy, M. Mohammed, H. Elsaedy, & I. Yahia, "Synthesis, optical limiting and properties of Rhodamine B-doped PMMA polymeric films/glass substrate: New trends in polymeric composites," *Optik*, vol. 212, p. 164687, 2020, <https://doi.org/10.1016/j.ijleo.2020.164687>
- [28] S. Brojabasi, & J. Philip, "Magnetic field dependant backscattering of light in water based ferrofluid containing polymer covered Fe<sub>3</sub>O<sub>4</sub> nanoparticles," *Journal of Applied Physics*, vol. 113, no. 5, p. 054902, 2013, <https://doi.org/10.1063/1.4789970>
- [29] S. H. Lafta, "Evaluation of hematite nanoparticles weak ferromagnetism," *Journal of Superconductivity and Novel Magnetism*, vol. 33, no. 12, pp. 3765–3772, 2020, <https://doi.org/10.1007/s10948-020-05626-8>
- [30] h. Mamiya, H. Fukumoto, J. L. C. Huaman, K. Suzuki, H. Miyamura, & B. Jeyadevan, "Estimation of magnetic anisotropy of individual magnetite nanoparticles for magnetic hyperthermia," *ACS Nano*, vol. 14, no. 7, pp. 8421–8432, 2020, <https://doi.org/10.1021/acsnano.0c02521>
- [31] P. Zu, C. C. Chan, T. Gong, Y. Jin, W. C. Wong, & X. Dong, "Magneto-optical fiber sensor based on bandgap effect of photonic crystal fiber infiltrated with magnetic fluid," *Applied Physics Letters*, vol. 101, no. 24, p. 241118, 2012, <https://doi.org/10.1063/1.4772017>
- [32] S. H. Lafta, "Investigation of static shear stress in a suspension of CO<sub>0.2</sub>Ni<sub>0.8</sub>Fe<sub>2</sub>O<sub>4</sub> nanoparticles in sesame oil," *Ukrainian Journal of Physics*, vol. 68, no. 6, p. 412, 2023, <https://doi.org/10.15407/ujpe68.6.412>